GEOPHYSICAL RESEARCH LETTERS, VOL. 39, L03601, doi:10.1029/2011GL050366, 2012

Mechanism for export of sediment-derived iron in an upwelling regime

S. A. Siedlecki,[1] A. Mahadevan,[2] and D. E. Archer[1]

Received 15 November 2011; revised 6 January 2012; accepted 10 January 2012; published 11 February 2012.

[1] Model simulations performed with a three-dimensional, high-resolution, process study ocean model of eastern boundary upwelling systems are used to describe a mechanism that efficiently transports sediment-derived dissolved iron offshore in the subsurface through the bottom boundary layer (BBL) during downwelling-favorable wind events. In the model, sediment-derived iron accumulates in the BBL on the outer shelf when the winds are upwelling-favorable. When the wind reverses, the iron-laden BBL is mixed into the water column and transported offshore along isopycnals that intersect the bottom. Depending on the frequency of wind reversal, between 10–50% of the shelf sediment-derived iron flux is exported offshore through this previously unidentified subsurface pathway. If this mechanism operates on all coastal upwelling regimes, the global export of sediment-derived iron to the open ocean would be equivalent to ten times larger than the estimated source of dissolved iron from aerosols. **Citation:** Siedlecki, S. A., A. Mahadevan, and D. E. Archer (2012), Mechanism for export of sediment-derived iron in an upwelling regime, *Geophys. Res. Lett.*, *39*, L03601, doi:10.1029/2011GL050366.

1. Introduction

[2] Sources of the limiting micronutrient iron to the ocean include atmospheric dust from the continents, coastal ocean sediments and hydrothermal vents [*Johnson et al.*, 1997; *Bruland et al.*, 1994; *Elrod et al.*, 2004; *Tagliabue et al.*, 2010]. In the North Pacific, a subsurface maximum in particulate iron derived from continental shelf sediments extends offshore from eastern margins at a depth of approximately 200 meters [*Lam et al.*, 2006; *Lam and Bishop*, 2008]. Previous studies have focussed on the role of surface processes in exporting shelf sediment-derived iron to the open ocean [*Lam et al.*, 2006; *Johnson et al.*, 2005]. However, no mechanism has been identified for the subsurface lateral export of shelf sediment-derived iron.

[3] Shelf sediments have the potential to contribute as much dissolved iron to the open ocean as the deposition of dust from the atmosphere [*Moore and Braucher*, 2008; *Krishnamurthy et al.*, 2010]. Iron-rich sediments exist all along the west coast of the US [*Sawlan and Murray*, 1983; *Shaw et al.*, 1990; *Johnson et al.*, 1999], around river mouths of the US and South America [*Aller*, 1998, 2004; *Severmann et al.*, 2010], off the coast of Africa [*Compton et al.*, 2009; *Küster-Heins et al.*, 2010], and around the Southern Ocean [*Tagliabue et al.*, 2010]. A sedimentary source of iron is suggested by elevated iron concentrations found in the benthic boundary layer, but the rate of iron transport to the interior of the ocean depends on features of the coastal circulation that are poorly resolved in GCMs. Here we use a high-resolution process study ocean model (PSOM) [*Mahadevan et al.*, 1996a, 1996b], set in a region where iron leakage from sediments has been measured or inferred [*Elrod et al.*, 2004; *Chase et al.*, 2005; *Cullen et al.*, 2009] and is dynamically representative as an eastern boundary upwelling system [*Flament et al.*, 1985; *Mooers and Robinson*, 1984], to examine how dissolved iron escapes to the open ocean.

2. Methods

[4] Sediment-derived iron is released in the model from the sediments on the shelf, scavenged onto particles in the water column, and consumed by biological uptake in the euphotic zone, while being transported with the circulation. It is modeled as:

$$\frac{DFe}{Dt} = -Fe\lambda_{prod}e^{-\frac{z}{z_0}} - Fe\lambda_{scav} + \frac{\partial}{\partial z}\left(\kappa\frac{\partial Fe}{\partial z}\right) \qquad (1)$$

where

$$\kappa\frac{\partial Fe}{\partial z}\Big|_{z=z_b} = \Gamma_{seds}$$

and

$$\frac{D}{Dt} \equiv \frac{\partial}{\partial t} + u\frac{\partial}{dx} + v\frac{\partial}{\partial y} + w\frac{\partial}{\partial z}$$

The northward and eastward distances are denoted by x and y respectively, while z is the vertical coordinate, and t is time. The velocities u, v, w are in the x, y, z directions respectively.

[5] Here Fe is the dissolved concentration of iron in μmol m^{-3}, z is depth in meters, z_0 is 30 meters and represents the e-folding depth for light attenuation and defines the euphotic depth ($\sim$100m), Γ_{seds} is the dissolved flux of iron from the sediments in μmol Fe m^{-2} d^{-1}, λ_{prod} is the uptake rate of nitrogen by phytoplankton of 0.17 days^{-1} [*Elskens et al.*, 1997; *Harrison et al.*, 1996], λ_{scav} is the particle scavenging rate of 10^{-5} day^{-1} [*Moore and Braucher*, 2008], and κ is the vertical diffusivity from the Mellor-Yamada v2.5 turbulence closure scheme. Γ_{seds} is estimated from the observed relationship between oxidation of organic carbon and dissolved flux of iron from the sediments. Γ_{seds} has a value of 2.22 μmol Fe m^{-2} d^{-1} on the shelf, assuming the rate of oxidation of organic carbon is 4 g C m^{-2} d^{-1} [*Elrod et al.*,

[1]Department of Geophysical Sciences, University of Chicago, Chicago, Illinois, USA.
[2]Woods Hole Oceanographic Institution, Woods Hole, Massachusetts, USA.

0094-8276/12/2011GL050366

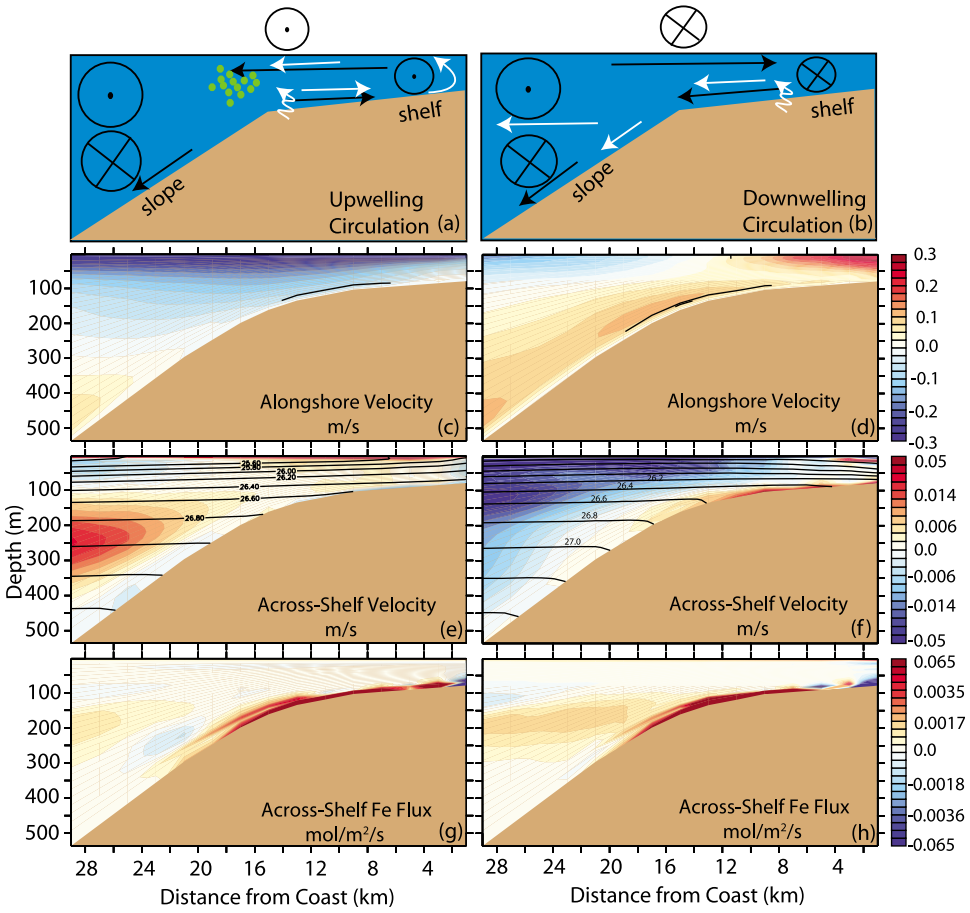

Figure 1. Mean circulation from the model forced by oscillating winds with a ten-day period. The results from time-averaged sections (left) during upwelling-favorable winds only, and (right) during downwelling-favorable winds only. (a, b) A schematic depiction of the mean circulation and mechanism for iron export from the shelf to slope waters. Circles with dots indicate equatorward flow and circles with crosses indicate poleward flow. Black arrows indicate mean cross-shelf flow, while white arrows indicate the response of the sediment-derived iron tracer. (c, d) Alongshore flow that is time-averaged during up-/down-welling wind periods, respectively, with contours of the 0.00001 s^{-1} vertical shear in the bottom boundary layer overlaid. Red colors indicate poleward flow, while blue colors indicate equatorward flow. (e, f) Across-shelf velocity with density contours overlaid. Red (warm colors) indicate offshore flow, blue colors indicate shoreward flow. Across-shelf flux of iron $v'c'_{Fe}$ averaged over (g) upwelling-favorable and (h) downwelling-favorable wind events. Here v' and c'_{Fe} are the perturbation of the cross-shelf velocity and sediment-derived iron from their average values calculated over periods when the winds are upwelling- and downwelling-favorable for Figures 1g and 1h, respectively.

2004; *Berelson et al.*, 2003]. Sensitivity studies to the chosen parameters are discussed in the auxiliary material.[1] Remineralization of organic material as a source of iron is not considered, because the goal is to determine the fate of the dissolved sediment-derived iron on the shelf. The model is initialized with no iron.

[6] The iron tracer is implemented in (PSOM), configured to a coastal setting in a periodic channel [*Siedlecki et al.*, 2011; *Lathuilière et al.*, 2010] for an upwelling oceanic front at 42°N. Our model uses an idealized topography with a narrow shelf and steep continental slope representative of eastern boundary upwelling systems. The domain is periodic in the alongshore direction. The model is initialized with measured density profiles and run for 350 days. Alongshore winds, which have a much greater effect on the circulation than cross-shore winds, are oscillated sinusoidally in time from poleward to equatorward for one set of experiments, and specified from observations in another. Both idealized and realistic wind stress are applied uniformly in space, except for the offshore boundary where it tapers to zero over 20 km. The idealized winds oscillate sinusoidally in time between poleward and equatorward with periods between 2 and 15 days and an amplitude of 0.1 N m^{-2}. The realistic winds are taken from buoy data (NDBC). A constant barotropic pressure gradient is imposed uniformly everywhere to drive the poleward undercurrent on the shelf. Further discussion can be found in the auxiliary material.

3. Results

[7] The model captures many of the features of eastern boundary upwelling system dynamics (Figure 1). For example, when the winds are equatorward (upwelling-favorable), offshore Ekman transport at the surface drives upwelling of dense waters on the shelf with lighter water offshore,

[1]Auxiliary materials are available in the HTML. doi:10.1029/2011GL050366.

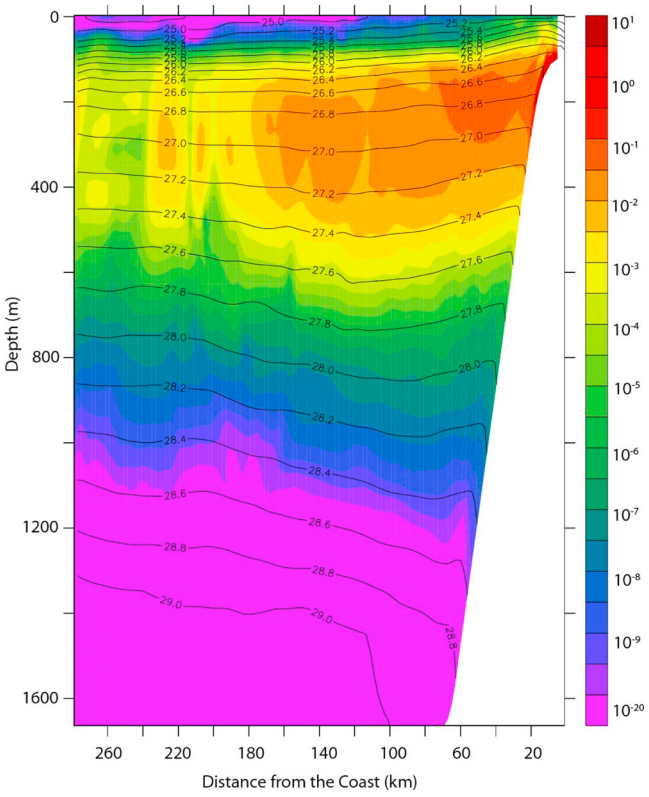

Figure 2. Sediment-derived iron tracer concentration in μmol m^{-3} or nM for a cross-section of the model domain, time-averaged over downwelling-favorable wind periods from the 10-day oscillating wind case, plotted on a log scale. Density (sigma) contours in black have a contour interval of 0.2.

generating equatorward flow on the shelf, and onshore flow in the BBL. When the winds shift to poleward (downwelling-favorable), flow on the shelf reverses to poleward, and flow in the BBL reverses to offshore [*Perlin et al.*, 2005; *Kurapov et al.*, 2005; *Lentz and Trowbridge*, 1991]. On the slope, however, surface equatorward flow overlies an alongshore poleward undercurrent [*Hill et al.*, 1998], regardless of the wind direction. The poleward undercurrent is driven by a basin-scale pressure gradient and is a ubiquitous feature of slope circulations in upwelling regimes [*Hill et al.*, 1998]. Its position and strength, which affect the export of iron, vary in response to the wind. The poleward undercurrent resides at ~150 m to 250 m below the surface in our model depending on the winds, deeper than in the seasonally averaged observations of *Pierce et al.* [2000] from the west coast of the US, which show it at ~100 m depth, but its strength is consistent with observations.

[8] In the model, the interaction between the alongshore flow on the slope and the frictional BBL plays an integral role in carrying dissolved and suspended iron offshore, into the interior of the ocean. Sediment-derived iron accumulates in the BBL on the outer shelf and upper slope during upwelling events. When the winds relax or reverse (to downwelling favorable), the vertical shear near the bottom boundary extends further offshore and the BBL thickens due to mixing [*Perlin et al.*, 2005]. The alongshore current on the shelf reverses to poleward and merges with the poleward undercurrent, which unifies the offshore flow in the frictional BBL on the shelf and slope [*Perlin et al.*, 2005; *Kurapov et al.*, 2005; *Hill et al.*, 1998] carrying sediment-derived iron off the shelf (Figures 1d and 1f).

[9] Once on the upper slope, an iron plume begins to detach from the BBL and spread offshore along isopycnal surfaces that intersect the bottom boundary near the top of the continental slope (Figure 1h). The plume (Figure 2) conveys the sediment-derived iron, and resides between the equatorward surface current and the poleward undercurrent. The vertical shear generated by the alongshore flow on the upper slope (shown by thin black lines in Figures 1c and 1d) extends further offshore during downwelling-favorable winds and enhances the vertical mixing of the BBL pool of sediment-derived iron, thereby facilitating its offshore transport.

[10] Our model receives a constant flux of iron from shelf sediments into the BBL, which can then be scavenged onto particles [*Moore and Braucher*, 2008], or taken up by phytoplankton near the surface. The model was not designed to reproduce the iron concentration profiles in the ocean, which are governed by the large-scale circulation and the global ocean iron cycle, but rather, to investigate the fate of a sediment-derived perturbation to the open-water offshore iron concentration profile. Our model simulates the transient evolution of the sedimentary iron; a steady state is not achievable on the relatively short space- and time-scales that are the focus here. Therefore, we evaluate the fate of shelf sediment-derived iron from the model output averaged over 100 days. Export and accumulation on the shelf are calculated using the rate of change in the inventory of iron on the slope and shelf, respectively.

[11] Because the total flux of iron from sediments is not well-constrained by observations [*Severmann et al.*, 2010], we present our estimate for shelf-derived iron export in terms of an export efficiency (E_χ), defined as the fraction of shelf sediment-derived iron transported beyond the shelf-slope break as shown in the following equation:

$$E_\chi = \frac{\int \left(\frac{dFe_{slope}}{dt} + Fe_{slope}\lambda_{prod}e^{-\frac{z}{z_0}} + Fe_{slope}\lambda_{scav} \right) dV_{slope}}{\int (\Gamma_{seds}) dA_{shelf}}.$$

We regard the transient build-up of dissolved iron in slope waters as the export flux of iron from the coast to the open ocean. We also include the uptake of dissolved iron by phytoplankton in the sunlit euphotic zone offshore of the continental shelf in our estimate of iron export to the open ocean iron cycle. Biological uptake in continental shelf waters, we assume, leads to redeposition of the iron in the sediments, and is consequently considered a loss of iron to the water column.

[12] In the oscillating wind scenario, the majority of the sediment-derived iron (~80%) is consumed by biological uptake on the shelf (Figure 3). The inventory of iron on the shelf increases over time in the model and is recorded as transient build-up (~4%) A small amount is scavenged on the shelf and slope (~0.05%). Accumulation in the slope waters accounts for 10% of the sediment flux, and about 10% is consumed by biological uptake on the slope. This results in an export efficiency (E_χ) of 0.2 for the case of

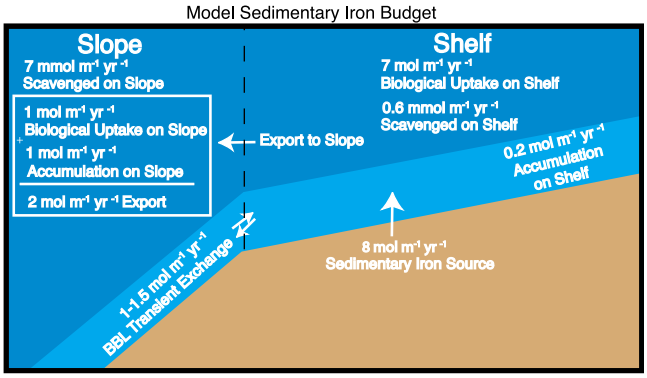

Figure 3. Model sedimentary iron budget for the oscillating wind scenario with a ten-day period. The majority of the sediment-derived iron is lost to production on the shelf. Export is considered to be the accumulation, as well as, the biological uptake, of iron on the slope. Units are mol per meter of coastline per year.

oscillating winds (Figure 3). During downwelling events, E_χ can be 0.9. During upwelling events, iron is upwelled onto the shelf, and iron is on the whole, lost from the open ocean, despite some returning to the open ocean as biological uptake on the slope, resulting in negative E_χ values ranging between −0.1 and −0.4 (Figures 4a and 4b). With symmetrically varying up- and down-welling favorable wind forcing, export from the shelf during downwelling events exceeds the return to the shelf during upwelling events, and E_χ is positive on average.

[13] Though the mean winds are upwelling-favorable in the summer, downwelling-favorable winds are a common occurrence, and dominate in the winter. Atmospheric forcing and sea surface temperature off the west coast of the US show significant variability on the 20–40 day timescales [*Bane et al.*, 2005, 2007]. Figure 4c shows the export efficiency for a model run forced with a wind stress record from the shelf off the coast of Newport, Oregon. Though the winds vary between up-/down-welling favorable, the export efficiency remains positive on average (time-averaged, $E_\chi = 0.5$ in Figure 3c).

[14] The export efficiency in the model is sensitive to the direction and duration of wind forcing events, and the mean wind direction. For winds that switch direction with periods between 2 and 15 days, we find that the shorter period in wind reversals result in more efficient offshore export of iron (Figure 4c). The longer the upwelling-favorable winds blow, the more iron is used for biological production on the shelf and the less available for subsurface export.

[15] Steady winds in either direction are inefficient at exporting iron. A mean upwelling-favorable wind forcing sets up an equatorward flow on the shelf, resulting in onshore transport in the BBL, and preventing iron export offshore. Mean downwelling-favorable winds are no more efficient in exporting iron than variable winds with no mean direction.

[16] Offshore iron transport is most efficient when the poleward undercurrent intersects the upper slope near the shelf break, and when the undercurrent is stronger, generating greater velocity shear on the slope (see auxiliary material). The current model design prevents investigation into the relative importance of the strength vs the depth of the undercurrent. In our model, adjusting either the mean alongshore wind stress or the imposed pressure gradient leads to changes in both the depth and the magnitude of the undercurrent on the slope.

4. Conclusions

[17] Assuming the continental shelves in upwelling regimes all experience a similar mechanism as the one described here

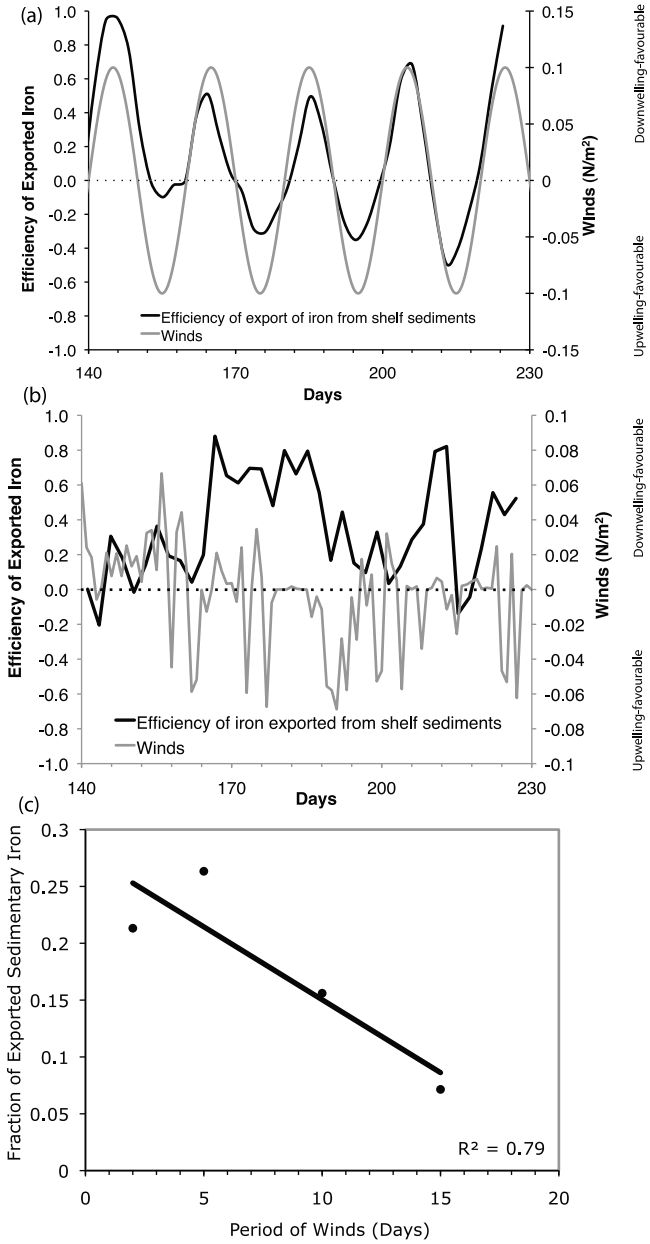

Figure 4. Efficiency of export of sediment-derived iron from the shelf (E_χ) over time. Downwelling-favorable winds are indicated as positive. (a) Ten-day oscillating wind case results. (b) Realistic wind forcing results. (c) Relationship between the period of the wind oscillation and the fraction of exported sediment-derived iron for four different oscillating wind scenarios with periods ranging from 2 to 15 days.

and export between 10–50% of the iron released from the sediments on the shelf, the amount of iron exported from shelves rivals the contribution from atmospheric dust deposition. *Elrod et al.* [2004] estimate the global flux of iron from sediments to be 8.9×10^{10} mol Fe yr^{-1} from the global average oxidation rate of organic carbon and the area for upwelling shelves (26,000,000 km^2). The efficiency of export in our model, in conjunction with this estimate of iron flux from sediments, suggests between 0.22 and 4×10^{10} mol Fe is exported to the open ocean from upwelling regimes per year.

[18] This flux is larger than that from hydrothermal vents, estimated to deliver for 9×10^8 mol Fe yr^{-1} globally [*Tagliabue et al.*, 2010], and smaller than total deposition from aerosols, estimated as $1–6 \times 10^{11}$ mol Fe yr^{-1} [*Fung et al.*, 2000; *Jickells and Spokes*, 2001]. Assuming 2% of the aerosols are soluble, the dissolved iron source would be between $2–12 \times 10^9$ mol Fe yr^{-1}. If the mechanism described here exists in all upwelling regimes, then the flux of iron from upwelling margins to the ocean interior is equivalent to ten times larger than the estimated dissolved flux from aerosols.

[19] **Acknowledgments.** We thank Burke Hales, Kipp Shearman, and Steve Ramp for their discussion on the physical circulation and Zanna Chase and Jim Moffett for discussion about iron in the coastal ocean. NSF supported this work. Correspondence and requests for materials should be addressed to Samantha Siedlecki (siedlesa@uw.edu).

[20] The Editor thanks Albert Hermann and an anonymous reviewer for their assistance in evaluating this paper.

References

Aller, R. C. (1998), Mobile deltaic and continental shelf muds as suboxic, fluidized bed reactors, *Mar. Chem.*, *61*(3–4), 143–155, doi:10.1016/S0304-4203(98)00024-3.

Aller, R. C. (2004), Conceptual models of early diagenetic process: The muddy seafloor as an unsteady, batch reactor, *J. Mar. Res.*, *62*(6), 815–835, doi:10.1357/0022240042880837.

Bane, J. M., M. D. Levine, R. M. Samelson, S. M. Haines, M. F. Meaux, N. Perlin, P. M. Kosro, and T. Boyd (2005), Atmospheric forcing of the Oregon coastal ocean during the 2001 upwelling season, *J. Geophys. Res.*, *110*, C10S02, doi:10.1029/2004JC002653.

Bane, J. M., Y. H. Spitz, R. M. Letelier, and W. T. Peterson (2007), Jet stream intraseasonal oscillations drive dominant ecosystem variations in Oregon's summertime coastal upwelling system, *Proc. Natl. Acad. Sci. U. S. A.*, *104*, 13,262–13,267, doi:10.1073/pnas.0700926104.

Berelson, W., J. McManus, K. Coale, K. Johnson, D. Burdige, T. Kilgore, D. Colodner, F. Chavez, R. Kudela, and J. Boucher (2003), A time series of benthic flux measurements from Monterey Bay, CA, *Cont. Shelf Res.*, *23*, 457–481, doi:10.1016/S0278-4343(03)00009-8.

Bruland, K. W., K. J. Orians, and J. P. Cowen (1994), Reactive trace metals in the stratified central North Pacific, *Geochim. Cosmochim. Acta*, *58*(15), 3171–3182, doi:10.1016/0016-7037(94)90044-2.

Chase, Z., B. Hales, T. Cowles, R. Schwartz, and A. van Geen (2005), Distribution and variability of iron input to Oregon coastal waters during the upwelling season, *J. Geophys. Res.*, *110*, C10S12, doi:10.1029/2004JC002590.

Compton, J., H. Caren, and R. Schneider (2009), Organic-rich mud on the western margin of southern Africa: Nutrient source to the Southern Ocean?, *Global Biogeochem. Cycles*, *23*, GB4030, doi:10.1029/2008GB003427.

Cullen, J. T., M. Chong, and D. Ianson (2009), British Columbian continental shelf as a source of dissolved iron to the subarctic northeast Pacific Ocean, *Global Biogeochem. Cycles*, *23*, GB4012, doi:10.1029/2008GB003326.

Elrod, V. A., W. M. Berelson, K. H. Coale, and K. S. Johnson (2004), The flux of iron from continental shelf sediments: A missing source for global budgets, *Geophys. Res. Lett.*, *31*, L12307, doi:10.1029/2004GL020216.

Elskens, M., W. Baeyens, and L. Goeyens (1997), Contribution of nitrate to the uptake of nitrogen by phytoplankton in an ocean margin environment, *Hydrobiologia*, *353*, 139–152, doi:10.1023/A:1003058928157.

Flament, P., L. Armi, and L. Washburn (1985), The evolving structure of an upwelling filament, *J. Geophys. Res.*, *90*(C6), 11,765–11,778, doi:10.1029/JC090iC06p11765.

Fung, I. Y., S. K. Meyn, I. Tegan, S. C. Doney, J. G. John, and J. K. G. Bishop (2000), Iron supply and demand in the upper ocean, *Global Biogeochem. Cycles*, *14*(1), 281–295, doi:10.1029/1999GB900059.

Harrison, W. G., L. R. Harris, and B. D. Irwin (1996), The kinetics of nitrogen utilization in the oceanic mixed layer: Nitrate and ammonium interactions at nanomolar concentrations, *Limnol. Oceanogr.*, *41*(1), 16–32, doi:10.4319/lo.1996.41.1.0016.

Hill, A. E., et al. (1998), Eastern ocean boundaries, in *The Sea*, vol. 11, *The Global Coastal Ocean: Regional Studies and Syntheses*, edited by A. R. Robinson and K. H. Brink, pp. 29–67, John Wiley, Hoboken, N. J.

Jickells, T. D., and L. J. Spokes (2001), Atmospheric iron inputs to the oceans, in *The Biogeochemistry of Iron in Seawater*, edited by D. R. Turner and K. A. Hunter, pp. 85–118, John Wiley, Hoboken, N. J.

Johnson, K. S., R. M. Gordon, and K. H. Coale (1997), What controls dissolved iron concentrations in the world ocean?, *Mar. Chem.*, *57*(3–4), 137–161, doi:10.1016/S0304-4203(97)00043-1.

Johnson, K. S., F. P. Chavez, and G. E. Friederich (1999), Continental-shelf sediment as a primary source of iron for coastal phytoplankton, *Nature*, *398*, 697–700, doi:10.1038/19511.

Johnson, W. K., L. A. Miller, N. E. Sutherland, and C. S. Wong (2005), Iron transport by mesoscale Haida eddies in the Gulf of Alaska, *Deep Sea Res., Part II*, *52*(7–8), 933–953, doi:10.1016/j.dsr2.2004.08.017.

Krishnamurthy, A., J. K. Moore, N. Mahowald, C. Luo, and C. S. Zender (2010), Impacts of atmospheric nutrient inputs on marine biogeochemistry, *J. Geophys. Res.*, *115*, G01006, doi:10.1029/2009JG001115.

Kurapov, A. L., J. S. Allen, G. D. Egbert, and R. N. Miller (2005), Modeling bottom mixed layer variability on the mid-Oregon shelf during summer upwelling, *J. Phys. Oceanogr.*, *35*(9), 1629–1649, doi:10.1175/JPO2768.1.

Küster-Heins, K., E. Steinmetz, and G. J. De Lange (2010), Phosphorus cycling in marine sediments from the continental margin off Namibia, *Mar. Geol.*, *274*(1–4), 95–106, doi:10.1016/j.margeo.2010.03.008.

Lam, P. J., and J. K. B. Bishop (2008), The continental margin is a key source of iron to the HNLC North Pacific Ocean, *Geophys. Res. Lett.*, *35*, L07608, doi:10.1029/2008GL033294.

Lam, P. J., J. K. B. Bishop, C. C. Henning, M. A. Marcus, G. A. Waychunus, and I. Y. Fung (2006), Wintertime phytoplankton bloom in the subarctic Pacific supported by continental margin iron, *Global Biogeochem. Cycles*, *20*, GB1006, doi:10.1029/2005GB002557.

Lathuilière, C., V. Echevin, M. Lévy, and G. Madec (2010), On the role of the mesoscale circulation on an idealized coastal upwelling ecosystem, *J. Geophys. Res.*, *115*, C09018, doi:10.1029/2009JC005827.

Lentz, S. J., and J. H. Trowbridge (1991), The bottom boundary-layer over the Northern California Shelf, *J. Phys. Oceanogr.*, *21*(8), 1186–1201, doi:10.1175/1520-0485(1991)021<1186:TBBLOT>2.0.CO;2.

Mahadevan, A., J. Oliger, and R. Street (1996a), A nonhydrostatic mesoscale ocean model. 1. Well-posedness and scaling, *J. Phys. Oceanogr.*, *26*(9), 1868–1880, doi:10.1175/1520-0485(1996)026<1868:ANMOMP>2.0.CO;2.

Mahadevan, A., J. Oliger, and R. Street (1996b), A nonhydrostatic mesoscale ocean model. 2. Numerical implementation, *J. Phys. Oceanogr.*, *26*(9), 1881–1900, doi:10.1175/1520-0485(1996)026<1881:ANMOMP>2.0.CO;2.

Mooers, C. N. K., and A. R. Robinson (1984), Turbulent jets and eddies in the California Current and inferred cross-shore transports, *Science*, *223*(4631), 51–53, doi:10.1126/science.223.4631.51.

Moore, J. K., and O. Braucher (2008), Sedimentary and mineral dust sources of dissolved iron to the world ocean, *Biogeosciences*, *5*(3), 631–656, doi:10.5194/bg-5-631-2008.

Perlin, A., J. N. Moum, and J. M. Klymak (2005), Response of the bottom boundary layer over a sloping shelf to variations in alongshore wind, *J. Geophys. Res.*, *110*, C10S09, doi:10.1029/2004JC002500.

Pierce, S. D., R. L. Smith, P. M. Kosro, J. A. Barth, and C. D. Wilson (2000), Continuity of the poleward undercurrent along the eastern boundary of the mid-latitude north Pacific, *Deep Sea Res., Part II*, *47*(5–6), 811–829, doi:10.1016/S0967-0645(99)00128-9.

Sawlan, J. J., and J. W. Murray (1983), Trace metal remobilization in the interstitial waters of red clay and hemipelagic marine sediments, *Earth Planet. Sci. Lett.*, *64*(2), 213–230, doi:10.1016/0012-821X(83)90205-4.

Severmann, S., J. McManus, W. M. Berelson, and D. E. Hammond (2010), The continental shelf benthic iron flux and its isotope composition, *Geochim. Cosmochim. Acta*, *74*(14), 3984–4004, doi:10.1016/j.gca.2010.04.022.

Shaw, T. J., J. M. Geiskes, and R. A. Jahnke (1990), Early diagenesis in differing depositional environments: The response of transition metals in pore water, *Geochim. Cosmochim. Acta*, *54*(5), 1233–1246, doi:10.1016/0016-7037(90)90149-F.

Siedlecki, S. A., D. E. Archer, and A. Mahadevan (2011), Nutrient exchange and ventilation of benthic gases across the continental shelf break, *J. Geophys. Res.*, *116*, C06023, doi:10.1029/2010JC006365.

Tagliabue, A., et al. (2010), Hydrothermal contribution to the oceanic dissolved iron inventory, *Nat. Geosci.*, *3*, 252–256, doi:10.1038/ngeo818.

D. E. Archer and S. A. Siedlecki, Department of Geophysical Sciences, University of Chicago, 5734 S. Ellis Ave., Chicago, IL 60637, USA. (siedlesa@uw.edu)

A. Mahadevan, Woods Hole Oceanographic Institution, 266 Woods Hole Rd., MS 29, Woods Hole, MA 02543, USA.